Materials Science and Engineering C 80 (2017) 494–501

Contents lists available at ScienceDirect

Materials Science and Engineering C

journal homepage: www.elsevier.com/locate/msec

Fabrication of biosensor based on Chitosan-ZnO/Polypyrrole nanocomposite modified carbon paste electrode for electroanalytical application

Amera Hassanein [a], Nehal Salahuddin [a], Atsunori Matsuda [b,*], Go Kawamura [b], Mona Elfiky [a,b]

[a] Department of Chemistry, Faculty of Science, Tanta University, Egypt
[b] Department of Electrical and Electronic Information Engineering, Toyohashi University of Technology, Japan

ARTICLE INFO

Article history:
Received 23 January 2017
Received in revised form 14 April 2017
Accepted 16 April 2017
Available online 18 April 2017

Keywords:
Polypyrrole
Zinc oxide nanoparticles
Chitosan
Sensor
Nanocomposite
Isoxsuprine HCl
Square-wave adsorptive anodic stripping voltammetry

ABSTRACT

A sensitive conductive nanocomposite sensor consisting of chitosan, zinc oxide nanoparticles, and polypyrrole was developed. The sensor was prepared by oxidative polymerization of pyrrole using $(NH_4)_2S_2O_8$ as the oxidant followed by mixing a Chitosan-Zinc oxide composite with a different content of Chitosan. The morphology and surface area of the nanocomposites were changed by changing the percentage of chitosan. The newly developed nanocomposites also showed a significant improvement in electrical conductivity as mentioned from the cyclic voltammetry measurements of the $K_3[Fe(CN)_6]$ sample. A square-wave adsorptive anodic stripping voltammetry method successfully measured Isoxsuprine hydrochloride using different types of nanocomposite modified CPEs and showed a large enhancement of stripping peak current compared to bare CPE. Consequently, the proposed sensors proved to have a promissing feature for applications in biosensors.

1. Introduction

The usage of nanomaterials has provided clear improvement of the chemical, physical properties of materials that are suitable for application in medicine, chemical sensing, electrochemical sensing, electronics, biotechnology, biomedical and bioanalytical applications. Nanomaterials development in electrochemical sensors has been widely studied as an inexpensive method to specifically and sensitively detect a variety of analytes [1–3]. Another class of nanomaterials, such as nano/mesoporous carbon [4,5], nanoporous graphene [6], and mesopoous metals [7,8] materials have been interestingly studied for electrochemical sensing applications. In particular, organic–inorganic nanocomposite materials such as conductive polymers and oxide nanocomposites have been used in numerous fields of application; biosensors, gas sensors, conductive paints, drug delivery, and rechargeable batteries [9–12] due to the novel properties of nanocomposite which can be derived from the successful blending of the characteristics of the parent constituents into a single material. The main properties of metal nanoparticles (NPs) such as zinc oxide (ZnO), titanium oxide (TiO_2), and silver oxide (Ag_2O), are mostly characterized by their size, composition, crystallinity, and morphology. The nanoscale size of these metal oxides generally confers larger surface areas compared with macro-sized particles [13] and is useful to modify their chemical, mechanical, electrical, structural, morphological, and optical properties. Moreover, these nanostructured materials have a larger percentage of surface atoms possessing high reactivity. ZnO NPs have been exploited as a potential material for biosensing and gas sensing because they have several marvellous properties, including a wide band gap (3.37 eV), high isoelectric point (IEP) of ~9.5, biocompatibility, nontoxicity, good selectivity, high catalytic efficiency, chemical stability, hydrophilicity, and strong adsorption ability [14–17]. ZnO NPs also have high surface area which enhances the interaction between materials and analytes, leading to high sensitivity, and their small dimensions enable fast adsorption/desorption kinetics for analytes in the material, which allows a rapid response time. Different synthesis methods have been devised for ZnO NPs with different morphology [18–24] such as vapor transport process [25], spray pyrolysis [26], hydrothermal synthesis [27], thermal decomposition [28], direct precipitation [29–31] and sol-gel processing [32,33]. The precipitation method in particular has been successfully used to design different structures of ZnO NPs [34]. Conducting polymers are useful nanocomposite of an electrochemical sensor. Polypyrrole (Ppy) is considered to be one of the best organic conducting polymers due to its excellent conductivity, having environmental stability and easy synthesis [35]. Ppy has been performed in a number of applications, such as in batteries,

* Corresponding author.
E-mail address: matsuda@ee.tut.ac.jp (A. Matsuda).

http://dx.doi.org/10.1016/j.msec.2017.04.101
0928-4931/

supercapacitors, sensors, corrosion protection and microwave shielding [36–39]. However, a direct combination of ZnO NPs and Ppy is inadequate to maintain the nanostructure and high stability in air because the interface is generally very sensitive to humidity [40]. Therefore, another support is required to combine ZnO NPs and Ppy effectively. Chitosan has special characteristics, such as biocompatibility, bioactivity, non-antigenicity and nontoxicity [41], and the membrane can include metal ion and organic materials [42]. Therefore, it has potential as a binder between ZnO NPs and Ppy [43]. In this paper, we developed a novel sensitive conductive nanocomposite sensor consisting of polypyrrole, ZnO NPs, and chitosan for detection of Isoxsuprine hydrochloride (IS·HCl) which is structured chemically as 4-{1-hydroxy-2-[(1-phenoxypropan-2yl) amino]propyl} phenol and used as a vasodilator [44] in humans and equines. IS·HCl is a β-adrenergic agonist that causes direct relaxation of uterine and vascular smooth muscle via β-2 receptors [45]. The ternary nanocomposite was designed not only to have high conductivity and a large surface area, but also to work as a selective adsorbent for an organic drug by the modification of the hydrophobicity of chitosan. In practice, the carbon paste electrode including the ternary nanocomposite demonstrated a selective adsorptive property beyond ZnO NPs as the electrochemical sensor [46].

2. Experimental work

2.1. Materials and solutions

All reagents were of commercial grade, and were used without further purification. Zinc nitrate hexahydrate "$Zn(NO_3)_2.6H_2O$, 99% Sigma-Aldrich", sodium carbonate "Na_2CO_3, 99% Sigma-Aldrich", Ethanol (C_2H_5OH, 95%, Pio chem.), high molecular weight chitosan "Sigma-Aldrich", "Pyrrole 98% Sigma-Aldrich". Other chemicals used were guaranteed grade. IS·HCl was purchased from Sigma, (Saint Louis, MO, USA). Britton–Robinson (B–R) universal buffer pH 6 was prepared in deionized water, and used as a supporting electrolyte.

2.2. Instruments

Fourier transform infrared (FTIR) spectra were measured by a Perkin Elmer spectrophotometer using the KBr disc technique in a wavenumber range of 4000–400 cm^{-1}. Wide angle X-ray diffraction (XRD) measurements were recorded, using a Phillips Powder-Diffractometer equipped with a Ni-filtered Cu-K_α ($\lambda = 1.5418$ Å), at a scanning speed of 2°/s. The samples were dried in a vacuum oven at 80 °C for 12 h, and then mounted on a sample holder with a large cavity. A smooth surface was obtained by pressing the powder samples with a glass plate. Bragg's Law ($n\lambda = 2d\sin\theta$) was used to compute the crystallographic spacing. JEOL JSM 5400 Scanning electron microscopy (SEM) was used to observe the particle morphologies of ZnO NPs and CS-ZnO/Ppy nanocomposites and modified Carbon paste electrodes (CPEs). Transmission electron microscopy (TEM) micrographs were obtained with a JEOL JEM-100CX electron microscope at an accelerating voltage of 100 KV. The film was prepared from samples dispersed in water. The surface areas of the samples were determined by Brunauer–Emmett–Teller (BET) N_2

Table 1
Preparation of nanocomposite modified CPEs.

Sample code	Nanocomposites Wt. (gm)	Carbon Wt. (gm)
Bare CPE	–	5
10%(w/w) [ZnO NPs] CPE	0.5	4.5
1%(w/w) [7.5% CS-ZnO/Ppy] CPE	0.05	4.95
1%(w/w) [15% CS-ZnO/Ppy] CPE	0.05	4.95
1%(w/w) [25% CS-ZnO/Ppy] CPE	0.05	4.95

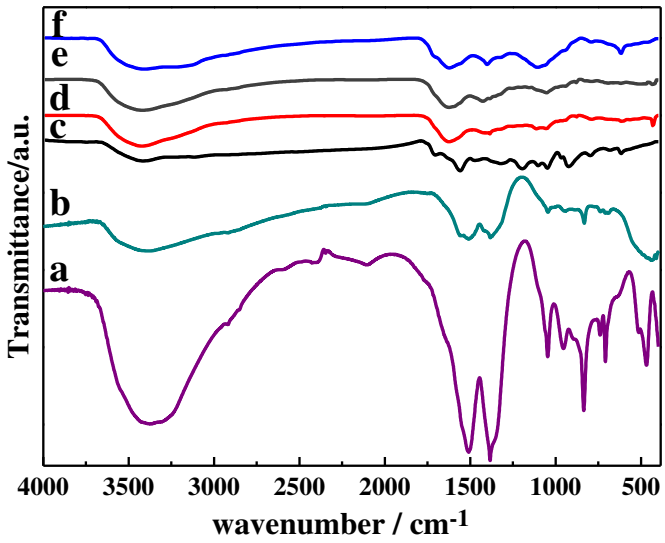

Fig. 1. FTIR of (a) $ZnCO_3$, (b) ZnO NPs, (c) [CS/Ppy], (d) [7.5% CS-ZnO/Ppy], (e) [15% CS-ZnO/Ppy], and (f) [25% CS-ZnO/Ppy] nanocomposites in the region 4000–400 cm^{-1}.

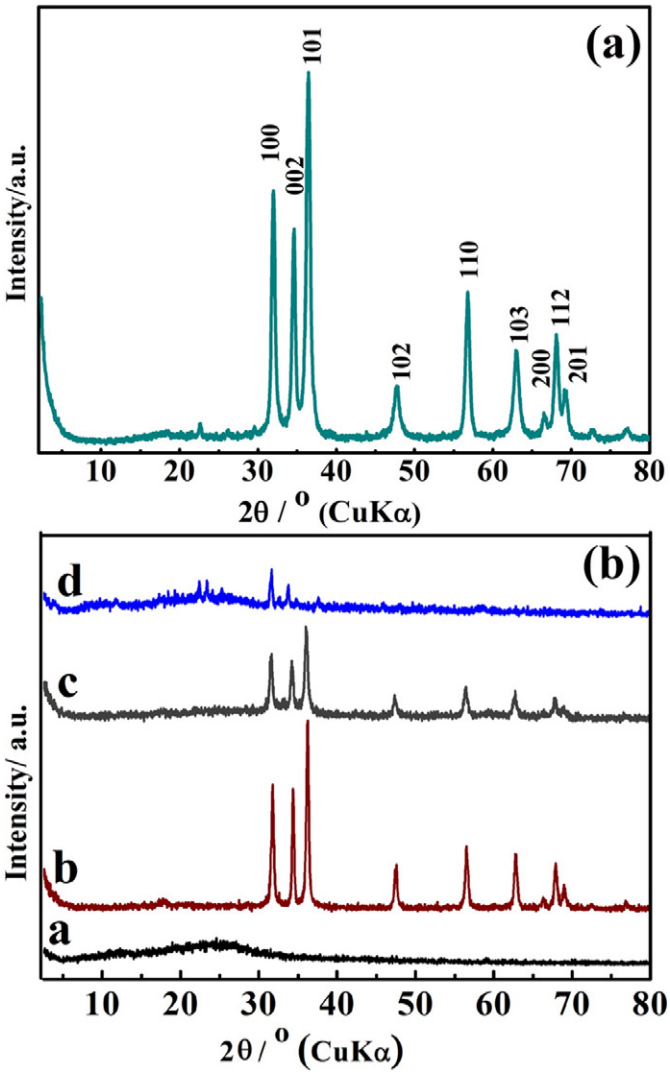

Fig. 2. XRD of (a) ZnO NPs, (b) (a) [CS/Ppy], (b) [7.5% CS-ZnO/Ppy], (c) [15% CS-ZnO/Ppy], and (d) [25% CS-ZnO/Ppy] nanocomposites.

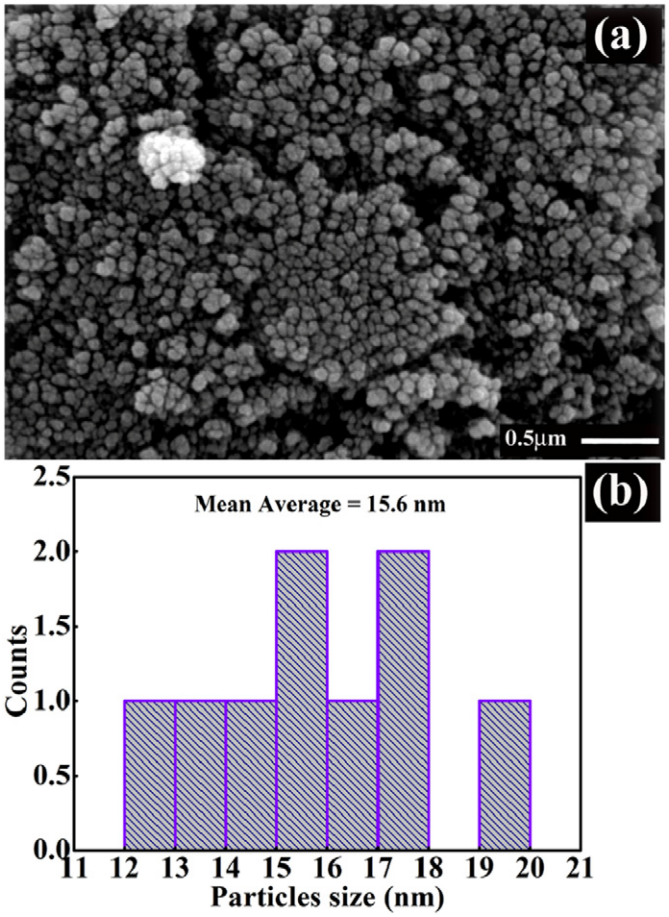

Fig. 3. SEM images of (a) ZnO NPs, and (b) histogram of particle size. The inset histogram shows the particle size.

sorption isotherms [TriStar II 3020 adsorption analyzer (Micromeritics, Norcross, USA)]. Samples were degassed at 120 °C, for 2 h under vacuum, prior to measurement. While, for voltammetric measurements computer-controlled potentiostats (PAR) Models 273A were used for analytical voltammetric peaks response.

2.3. Preparation of zinc oxide nanoparticles

For preparing a $ZnCO_3$ precursor, 200 mL of 0.1 mol/L of $Zn(NO_3)_2$ solution was slowly dropped into a vigorously stirred 240 mL of 0.1 mol/L of Na_2CO_3 solution with a molar ratio of 1:1.2. After addition, the precipitate was collected by filtration and repeatedly rinsed with high-purity water, ethanol and dried at 100 °C for 6 h, respectively. Finally, the precursor was annealed in the muffle furnace in the temperature 350 °C for 2 h to obtain the ZnO NPs [47].

2.4. Preparation of chitosan/polypyrrole material

A chitosan solution was prepared as follows: 0.25 g of chitosan dissolved in 50 mL of 2% of acetic acid with vigorous stirring for 1 h. A polypyrrole solution was prepared by following: 0.68 g Pyrrole dissolved in 50 mL of 0.1 M acetic acid and was polymerized with 4.56 g of $(NH_4)_2S_2O_8$ in an ice bath for 1 h. Then the polypyrrole solution was slowly poured into the chitosan solution with stirring for 20 min, and settled for 24 h. Then precipitate [CS/Ppy] was filtered, washed with distilled water, and dried at 80 °C.

2.5. Preparation of chitosan-ZnO/polypyrrole nanocomposites

Preparation of [7.5% CS-ZnO/Ppy] nanocomposite was carried out as follows: After 2.5 g of ZnO NPs was sonicated in 50 mL of distilled water, (0.25 g in 50 mL) of the chitosan solution was added to ZnO dispersion with constant stirring at 80 °C, and allowed to settle for 24 h. The supernatant solution was discarded and the precipitate was rinsed with double distilled water several times. Then in an ice bath, the polypyrrole solution was slowly poured into the chitosan-ZnO precipitate while vigorously stirring for 20 min, and settled for 24 h, then washed with distilled water, and dried at 80 °C. The same procedure was carried out using 0.5 g and 1.0 g of chitosan to obtain [15% CS-ZnO/Ppy] and [25% CS-ZnO/Ppy], respectively.

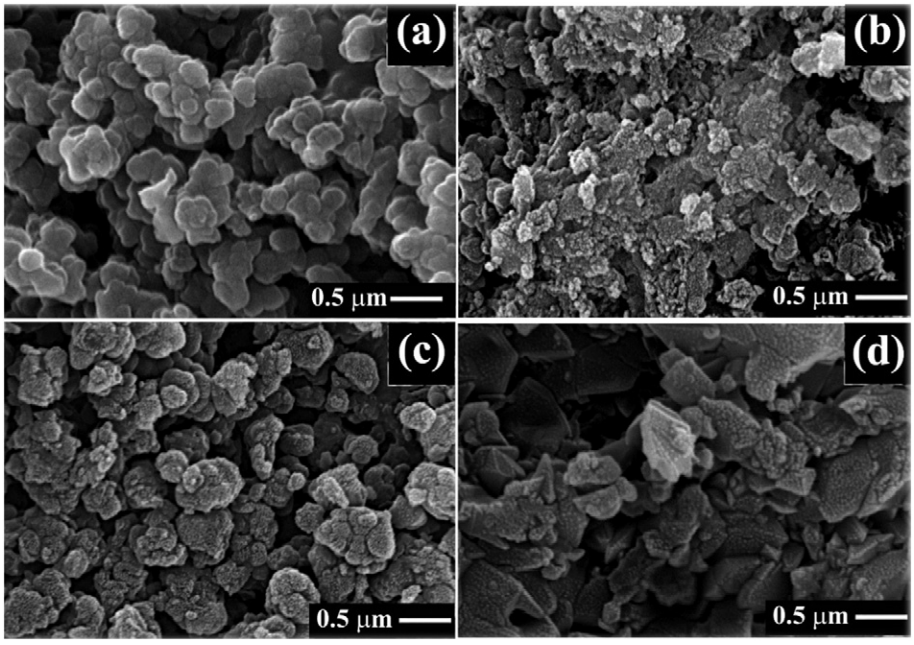

Fig. 4. SEM images of (a) [CS/Ppy], (b) [7.5% CS-ZnO/Ppy], (c) [15% CS-ZnO/Ppy], and (d) [25% CS-ZnO/Ppy] nanocomposites at the same magnification.

2.6. Preparation of modified carbon paste electrodes (CPEs)

Carbon paste (CP) was prepared by thoroughly mixing graphite powder (5.0 g) with paraffin oil (1.8 mL) in a carnelian mortar. The modification of CP with 1% (*w*/w) of prepared nanocomposites was carried out by mixing fine graphite powder (4.95 g) with different types of prepared nanocomposites (0.05 g) in a carnelian mortar, with sufficient paraffin oil (1.8 mL) to give a homogenous material. The same procedure was carried out with different amount of prepared nanoparticle and nanocomposites materials as shown in (Table.1). CPs were pressed into the end cavity of a working electrode (3 mm diameter), the electrode surface was smoothed with clean paper until shiny. Then the CP electrodes were immersed in a cell containing supporting electrolyte, and A square wave adsorptive anodic stripping voltammetry method was applied [48].

3. Results and discussion

3.1. Characterization of prepared nanocomposite materials

3.1.1. Fourier transform-infrared spectroscopy

FT-IR spectrum of $ZnCO_3$ is shown in Fig.1(a), the strong peaks at 1384 cm^{-1} and 1522 cm^{-1} are assigned to $ZnCO_3$, the absorption tape in the 713–1044 cm^{-1} range is due to the lattice vibration of the carbonate ion and a broad band at 3375 cm^{-1} was assigned to the stretching vibration mode of the hydroxyl group (—OH) [49–51]. This also proves that the precursor was zinc hydroxyl carbonate. After annealing of the precursor as shown in Fig.1 (b), a peak appeared at 457 cm^{-1} which was attributed to Zn—O stretching, and peaks at (1384 and 1522 cm^{-1}) shifted and reduced significantly to 1375 and 1507 cm^{-1} after annealing. While, the peak at 3375 cm^{-1} shifted and reduced significantly to 3433 cm^{-1} which confirmed the decomposition of the hydroxyl group. FTIR spectrum of [CS/Ppy] is shown in Fig.1 (c), the typical peak was observed at 3415 cm^{-1} could be assigned to the axial stretching vibration of O—H of chitosan superimposed to the N—H stretching band of pyrrole and inter hydrogen bonds of the polysaccharide which confirms the presence of strong hydrogen bonds between CS and Ppy; the peak at around 1562 cm^{-1} was assigned to the —C═C— stretch of the pyrrole ring, the peak at around 1318 cm^{-1} was caused by the a stretching vibration of C—N and the peak at 1098 cm^{-1} was caused by —N—H in-plane deformation of the pyrrole unit [52]. A peak at 1701 cm^{-1} is attributed to C═O (acetylated amino) stretching mode. While, a peak at 1051 cm^{-1}, which corresponded to the stretching vibration of C–O–C and the specific bands of the β (1–4) glycoside bridge at 1195 and 911.8 cm^{-1} were observed [52–55]. FTIR spectrum of the nanocomposites with different percentages of CS showed a broad absorption band centred between 3170 and 3415 cm^{-1} due to the overlap of N—H and OH stretching vibrations Fig.1 (d, e and f). This band was much broader than the band observed in the spectra of [CS/Ppy] due to the hydrogen bond with ZnO (N—H…O, and O—H…O). Also, the characteristic peak of ZnO NPs at 457 cm^{-1} which reduced, shifted to 430 cm^{-1} and then disappeared for the prepared nanocomposites. The peaks observed in the spectrum of Ppy/CS composite (at 1701 and 1318 cm^{-1}) shifted to 1619 and 1400 cm^{-1}, respectively. A similar shift was reported in the literature and was attributed to the formation of Ppy/ZnO/CS complexes [56–58].

3.1.2. X-ray diffraction spectroscopy

XRD pattern of ZnO NPs shows the peaks at 2θ = 31.98°, 34.60°, 36.45°, 47.78°, 56.80°, 63.02°, 66.86°, 68.13°, 69.23°, 72.92°, and 77.12° which, were assigned to (100), (002), (101), (102), (110), (103), (200), (112), (201), (004), and (202) of ZnO NPs indicating that the ZnO NPs formed (Fig.2(a) Zincite, JCPDS 36_1451) [59–61]. No characteristic peaks of any impurities were detected, suggesting that high quality ZnO NPs were synthesized [47]. The average crystalline size of ZnO NPs was calculated according to Scherer's equation with crystalline particle size of 14.74 nm. The XRD pattern of [CS/Ppy] showed a broad reflection at 25° indicating a highly amorphous structure [62,63]. The reflections characteristic to ZnO NPs in the XRD patterns (100, 002 and 101) confirm the presence of ZnO NPs [64]. Also, the presence of a broad peaks at 2θ = 12.02°, and 24.14° corresponding to CS/Ppy was observed at a high content of CS as seen in Fig. 2 (b)–(a).

3.1.3. Scanning electron spectroscopy

SEM image of ZnO NPs in Fig.3 (a) shows densely-aggregated nanoparticles with an average diameter of 15.6 nm (using Image.J program) as shown in Fig.3 (b). SEM micrograph of [CS/Ppy] in Fig.4 (a) shows aggregates of the particles forming cauliflower like structures. Examination of different percentage of the nanocomposites Figs.4 (b, c and d) did not reveal the inorganic aggregation and show a significant difference in overall morphology having very small protrusions at the surface. The [15%CS-ZnO/Ppy] nanocomposite shows a smart morphology, much like a coral reef shape with a very small protrusions morphology which confirm the presence of high surface areas Fig.4 (c). Also, a

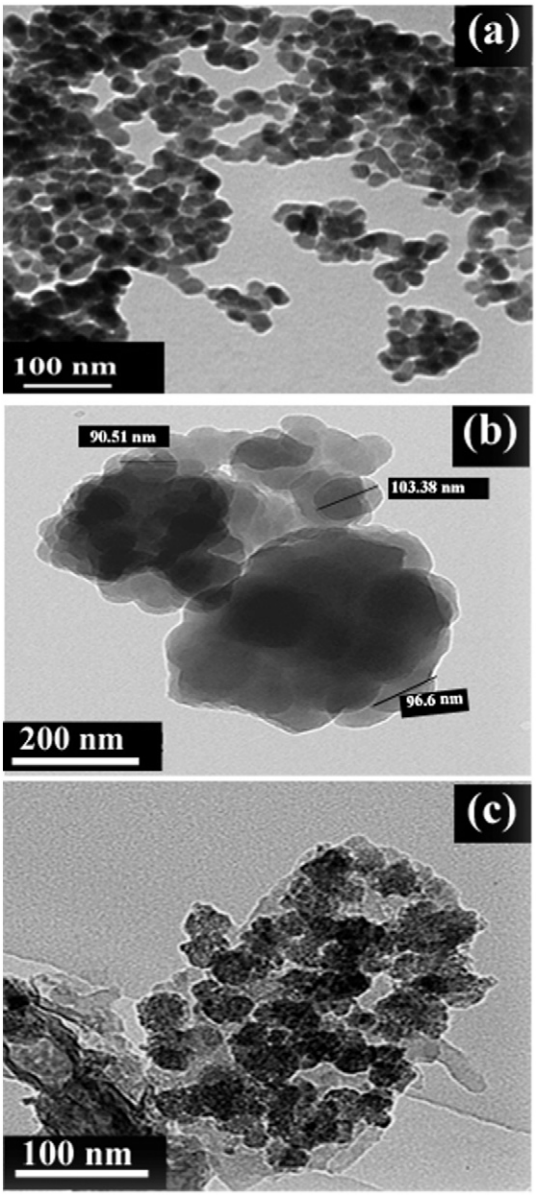

Fig. 5. TEM images of (a) ZnO NPs, (b) [CS/Ppy] nanocomposite, and (c) [15% CS-ZnO/Ppy] nanocomposite at the same magnifications.

uniform distribution of ZnO particles on the surface of Ppy/CS matrix was observed. However, the SEM images of [7.5%CS-ZnO/Ppy] and [25% CS-ZnO/Ppy] clearly show irregular morphology.

3.1.4. Transmission electron spectroscopy

TEM images Fig.5, show that the ZnO NPs are spherical in shape in Fig.5 (a) and the average diameter is 15.6 nm. It is worth mentioning that the average crystal diameter obtained from Scherer's formula 14.74 nm is in good agreement with the value obtained from analysis of the TEM images. It was reported that the application of Scherer's formula is restricted to small particles (usually smaller than 100 nm) [43]. Also, the TEM image of [CS/Ppy] shows a spherical shape with an average diameter of 96.9 nm Fig.5 (b). While, the TEM image of [15% CS-ZnO/Ppy] nanocomposite Fig.5 (c) shows irregular shape like-balls (bright areas) corresponding to [CS/Ppy] structure with the presence of dark areas inside it which corresponds to ZnO NPs with average size of 9.5 nm. This TEM image confirms the dispersion of ZnO NPs into the matrix of CS/Ppy with a new morphology.

3.1.5. Surface area and porosity analysis by BET/N_2

Adsorption isotherms were analysed with BET/N_2, as shown in Fig.6 for further investigation of the surface property of the as-prepared nanocomposites. The nanocomposites show isotherms nearly to a type IV isotherm which has a hysteresis loop in a relative pressure (P/P_0) range of 0.6–1.0 which indicates the existence of mesoporous structures in the synthesized nanostructures and the initial part of isotherm related to adsorption isotherm of type III [65]. Furthermore, obvious H_3 hysteresis loops were observed, indicating the formation of slit-like pores by stacking sheet-like [66,67]. The BET analysis revealed that the [15% CS-ZnO/Ppy] has the highest specific surface area 34.8 m^2/g with respect to other prepared nanocomposites which are summarized as the follows: 40.7, 14.6, 4.37, 18.96, and 7.01 m^2/g for $ZnCO_3$, ZnO NPs, [CS/Ppy], [7.5% CS-ZnO/Ppy], and [25% CS-ZnO/Ppy], respectively. Also, the pore size distribution determined by the Dollimore-Heal (DH) method as inset Fig.6, showed non-uniform pores in the range of 5–40 nm in diameter for all prepared materials. The high BET specific surface area and mesoporous structure can enhance electron and ion transport, resulting in high electrochemical capacity for the nanocomposite [65,68–73].

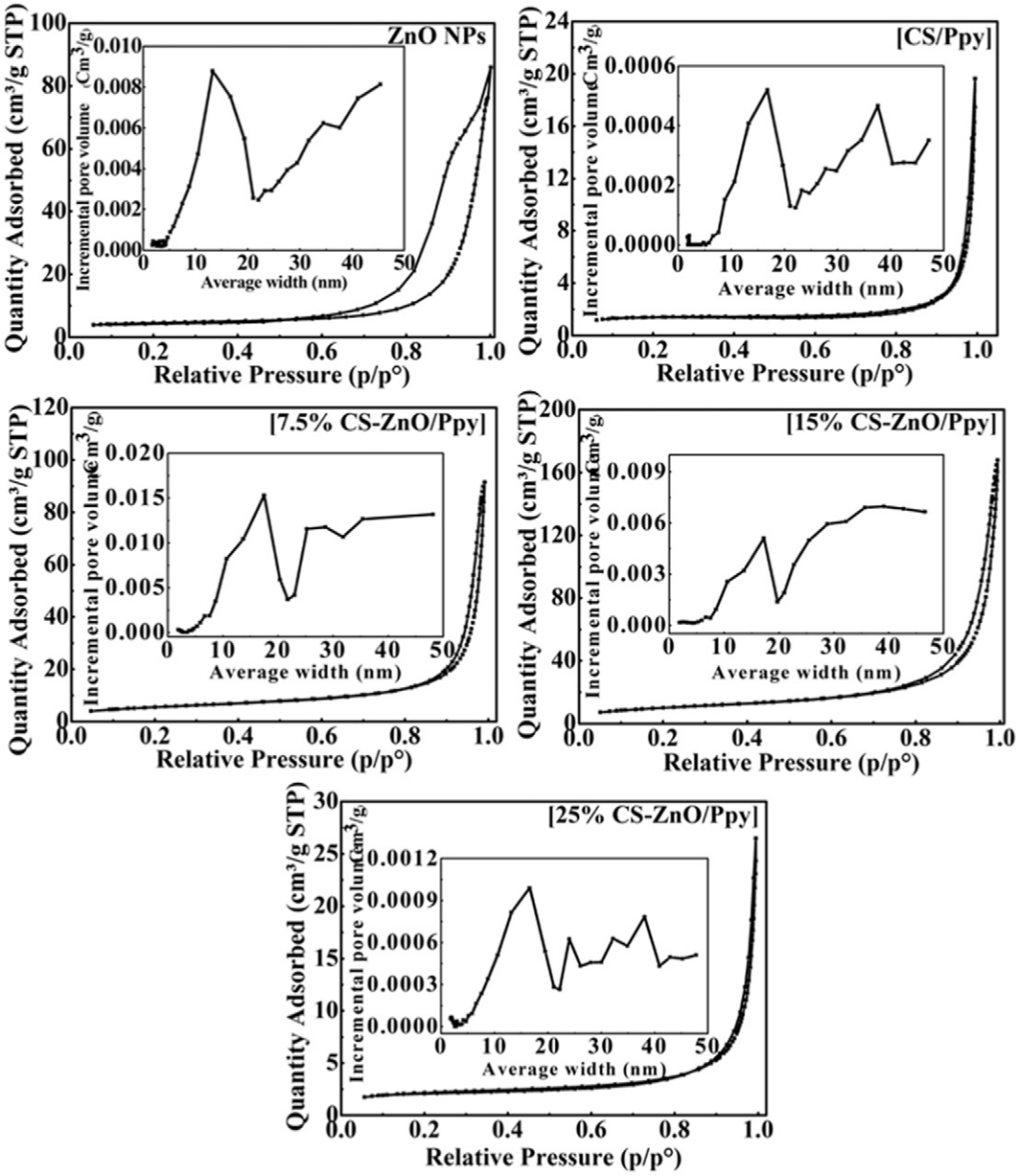

Fig. 6. N_2 adsorption-desorption isotherms for different materials, and Dollimore-Heal (DH) method for pore size distribution.

3.2. Electrochemical behavior of different types of biosensors

The cyclic voltammetry behaviors of 5×10^{-3} mol.L^{-1} $K_3[Fe(CN_6)]$ as an electroactive substance in 0.1 mol.L^{-1} of KCl using 10% (*w*/w) [ZnO NPs], 1% (*w*/w) [7.5% CS-ZnO/Ppy], 1% (*w*/w) [15% CS-ZnO/Ppy] and 1% (*w*/w) [25% CS-ZnO/Ppy] modified CPEs showed a pair of well-defined redox peak $I_{pa}/I_{pc} \approx 1.0$ (quasi-reversible peak) which is attributed to the transformation between $[Fe(CN)_6]^{4-}$ / $[Fe(CN)_6]^{3-}$ compared to Bare CPE as shown in Fig.7. The voltammograms showed a shift of the oxidation/reduction peak to more negative/positive potentials, respectively with (ΔE_p = 210, 200, 168 and 224 mV) for 10% (*w*/w) [ZnO NPs], 1% (*w*/w) [7.5% CS-ZnO/Ppy], 1% (*w*/w) [15% CS-ZnO/Ppy] and 1% (*w*/w) [25% CS-ZnO/Ppy] modified CPEs with respect to Bare CPE (ΔE_p = 246 mV), respectively. Whereas, the apparently smaller peak to peak separation (ΔE_p) may arise from the facilitated electron transfer of $[Fe(CN)_6]^{3-}$ pinholes in the structure of modified CPEs. However, the observed current response is significantly higher and the shape of the peak is much better defined. The peak current enhancement, accompanied with peak potential shift for all modified CPEs compared to Bare CPE suggests that the modified CPEs have higher electroanalytic activity compared with the Bare CPE.

It is noteworthy that, 1% (*w*/w) [15% CS-ZnO/Ppy] CPE is the highest in reversibility, electroactivity surface area and these results give a clear indication that 1% (*w*/w) [15% CS-ZnO/Ppy] CPE can be used as a very sensitive biosensor.

3.3. Electroanalytical behavior of different types of biosensors

A SW-AdAS voltammetric sensing of 8.0×10^{-8} mol/L IS·HCl using 10% (*w*/w) [ZnO NPs] CPE and 1% (*w*/w) of different types of [CS-ZnO/Ppy] as a modifier for CPE were successfully examined and compared with Bare CPE as shown in Fig.8. All nanocomposites modified CPEs showed large enhancement in peak current with respect to Bare CPE.

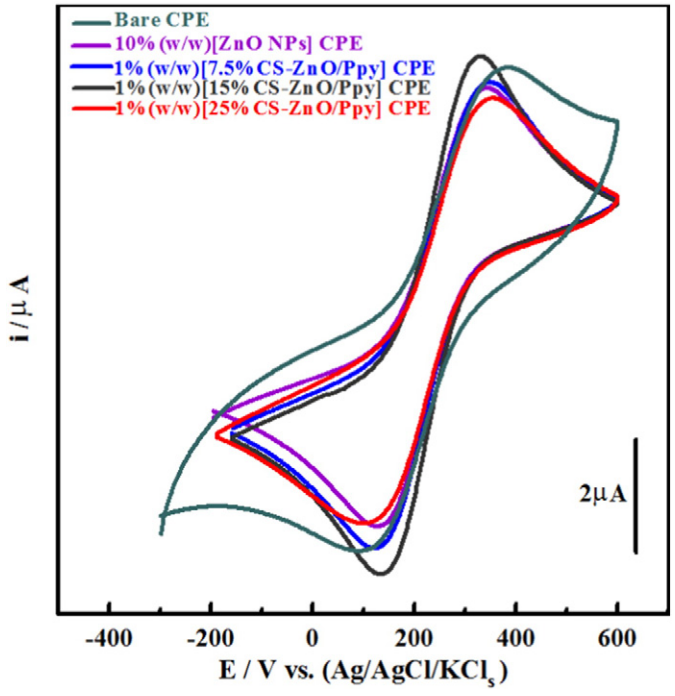

Fig. 7. Cyclic voltammograms of 5×10^{-3} mol.L^{-1} $K_3[Fe(CN)_6]$ in 0.1 mol.L^{-1} of KCl using (a) bare CPE, (b) 10% (*w*/w) [ZnO NPs] CPE, (c) 1%(*w*/w) [7.5% CS-ZnO/Ppy], (d) 1%(*w*/w) [15% CS-ZnO/Ppy], and (e) 1%(*w*/w) [25% CS-ZnO/Ppy] modified CPEs (scan rate of 200 mVs^{-1}).

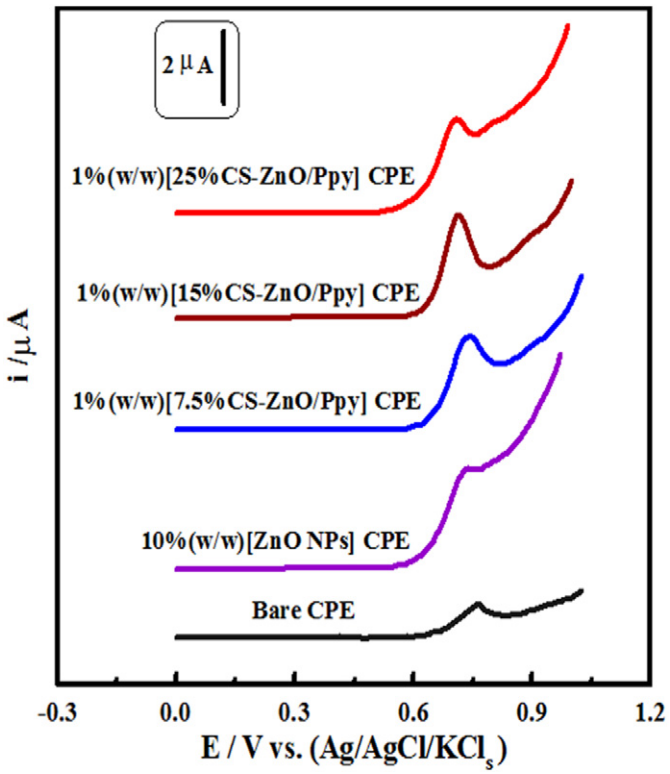

Fig. 8. SW-AdAS voltammograms of 8.0×10^{-8} mol.L^{-1} IS·HCl in the B-R universal buffer solution of pH 6 recorded following preconcentration by adsorptive accumulation at $E_{acc} = +0.0$ *V* for 15 s onto modified CPE with different types of modified CPEs (f = 80 H_z, a = 25 mV and ΔE_s = 9 mV).

It is noteworthy that, the 1% (*w*/w) [15% CS-ZnO/Ppy] CPE showed more affinity toward IS·HCl and about 366.6% increase in voltammetric signal with respect to Bare CPE (Table.2). These results revealed that nanocomposites have good catalytic and selectivity characteristics toward IS·HCl. Furthermore, the SEM morphology of the smooth surface of 10% (*w*/w) [ZnO NPs] and 1% (*w*/w) [(7.5–25) % CS-ZnO/Ppy] CPEs Figs.9 (a–d) revealed that 1% (*w*/w) [7.5% CS-ZnO/Ppy] and 1% (*w*/w) [25% CS-ZnO/Ppy] CPEs have very compact particles which decrease surface area Figs.9 (b and d) and this proved the decrease in the peak current intensity of voltammetric sensing Fig.8. While, the 1% (*w*/w) [15% CS-ZnO/Ppy] CPE Fig.9 (b) has small and smooth domains assembled in a necklace like structure which provide the largest surface area of CPE and greater improvement of adsorption and sensitivity for determination of IS·HCl compared with the other modified CPE electrodes. The stability of the modified electrode was studied during its storage in air at room temperature. The proposed sensor retained 96% of its initial activity for more than 14 days. These results indicate that the modified electrode has high stability. Moreover, the reproducibility, and repeatability of the proposed sensor toward IS·HCl detection were also investigated, and

Table 2
Effect of modification of CPE using the SW-AdAS voltammogram signal of 8.0×10^{-8} mol.L^{-1} IS·HCl in B-R buffer of pH 6.

Electrode	Peak current i_p (μA)	% of i_p of modified electrode with respect to Bare CPE
Bare CPE	0.60	100
10%(*w*/w)[ZnO NPs] CPE	1.12	186.6
1% (*w*/w) [7.5% CS-ZnO/Ppy] CPE	1.60	266.6
1% (*w*/w) [15% CS-ZnO/Ppy] CPE	2.2	366.6
1% (*w*/w) [25% CS-ZnO/Ppy] CPE	1.2	200.0

The highest in peak current percentage (Ip %).

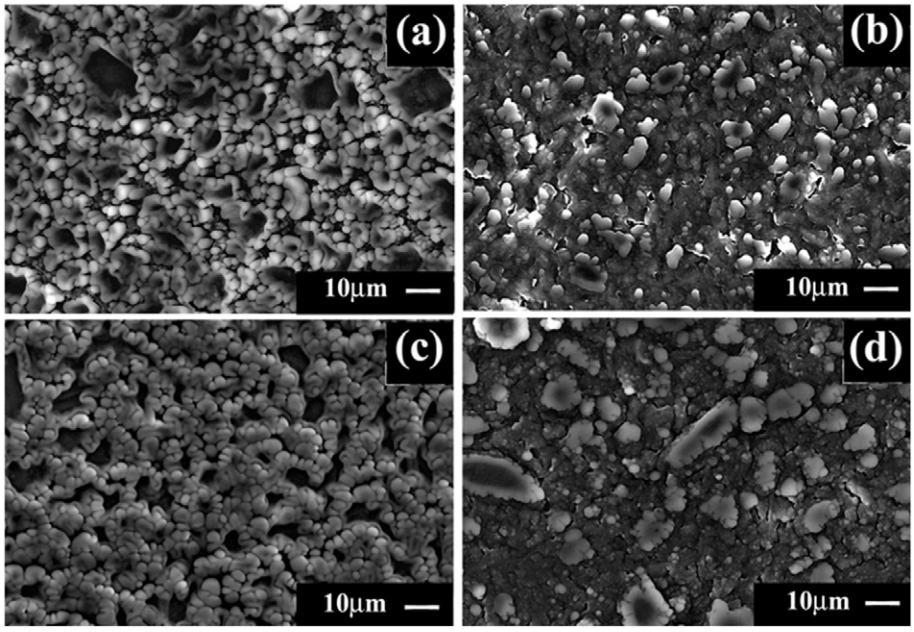

Fig. 9. SEM images of (a) 10% (*w*/w) [ZnO NPs], (b) 1%(*w*/w) [7.5% CS-ZnO/Ppy], (c) 1%(*w*/w) [15% CS-ZnO/Ppy], and (d) 1%(*w*/w) [25% CS-ZnO/Ppy] CPEs.

the standard deviation in the oxidation current were about 2.8, and 3.3% for successive measurements with 8.0×10^{-8} mol/L of IS·HCl, respectively.

These intriguing features of the nanocomposites and nanocomposite modified CPEs make them promising materials for applications as biosensors for electroanalytical measurements and [15% CS-ZnO/Ppy] as a modifier for CPE is the best of them. Under the operational conditions, SW-AdAS voltammograms of different concentrations of IS·HCl were recorded to achieve the linear regression equation as follows: I_{pa} (μA) = 31.3C + 0.175 (R = 0.998) using the bare CPE, and I_{pa} (μA) = 155.75C + 0.44 (R = 0.995) using the modified CPE, where I_{pa} was the anodic peak current (I, μA) and C was the IS·HCl concentration (C, nmol.L^{-1}). Further investigation of the electroanalytical measurements of IS·HCl in pharmaceutical and biological fluids using the CPE modified with ZnO NPs, and [15% CS-ZnO/Ppy] nanocomposite is currently on-going.

4. Conclusion

Novel nanocomposites which consist of Polypyrrole, zinc oxide nanoparticles, and chitosan were prepared by oxidative polymerization of pyrrole using $(NH_4)_2S_2O_8$ as an oxidant followed by mixing Chitosan-Zinc oxide composite with different amounts of chitosan. The different percentages of chitosan content in the nanocomposites revealed a marvelous difference in morphology, and evident change in specific surface area. A square wave adsorptive anodic stripping voltammetry method was tested for detection of IS·HCl using carbon paste electrode blended with a specific percentage of ZnO Nps and CS-ZnO/Ppy (with different concentration of CS). The voltammetric signals of proposed electrodes were compared with Bare CPE. The developed sensors revealed more selectivity, catalytic properties, and offer higher sensitivity compared to unmodified CPE.

These intriguing features of nanocomposites and nanocomposite modified CPEs make them promising materials for application as biosensors for electroanalytical measurements with [15% CS-ZnO/Ppy] modified CPE being the best of them. Details of electroanalytical measurements of IS·HCl using the CPE modified with [15% CS-ZnO/Ppy] nanocomposites will be discussed further later.

5. Acknowledgements

The authors are thankful for the Ministry of Higher Education, Cultural Affairs and Missions Sector, Egypt (E-568), for financially supporting the present work. This work has been partly supported by the Japan Society for the Promotion of Science (Grant-in-Aid for Scientific Research (A), No. 26249097).

References

[1] Y. Shao, J. Wang, H. Wu, J. Liu, I.A. Aksay, Y. Lin, Electroanalysis 22 (2010) 1027–1036.
[2] R.S. Dey, R.K. Bera, C. Raj, Anal. Bioanal. Chem. 405 (2013) 3431–3448.
[3] C. Zhu, G. Yang, H. Li, D. Du and Y. Lin, Anal. Chem. 87 (2014) 230–249.
[4] H.L. Poh, M. Pumera, Chem. Asian. J. 7 (2012) 412–416.
[5] M.M. Ghoneim, H.S. El-Desoky, A. Matsuda, T. Hattori, M.M. Abdel-Galeil, RSC Adv. 5 (2015) 56086–56097.
[6] W. Yuan, J. Chen, G. Shi, Mater. Today 17 (2014) 77–85.
[7] Y. Li, Y. Liu, Y. Yang, F. Yu, J. Liu, H. Song, J. Liu, H. Tang, B.-C. Ye, Z. Sun, ACS Appl. Mater. Interfaces 7 (2015) 15474–15480.
[8] D.M. Fouad, W.A. El-Said, J. Nanomater. (2016) 2016.
[9] D.I. Bower, An Introduction to Polymer Physics, Cambridge University Press, 2002.
[10] M. Butterworth, R. Corradi, J. Johal, S. Lascelles, S. Maeda, S. Armes, J. Colloid Interface Sci. 174 (1995) 510–517.
[11] M. Chougule, D. Dalavi, S. Mali, P. Patil, A. Moholkar, G. Agawane, J. Kim, S. Sen, V. Patil, Measurement 45 (2012) 1989–1996.
[12] Y.-C. Tsai, S.-C. Li, S.-W. Liao, Biosens. Bioelectron. 22 (2006) 495–500.
[13] B. Ashe, A Detail Investigation to Observe the Effect of Zinc Oxide and Silver Nanoparticles in Biological System, 2011.
[14] N. Guernion, B. de Lacy Costello, N.M. Ratcliffe, Synth. Met. 128 (2002) 139–147.
[15] J. Shi, Y. Zhu, X. Zhang, W.R. Baeyens, A.M. Garcia-Campaña, TrAC Trends Anal. Chem. 23 (2004) 351–360.
[16] J. Wang, X.W. Sun, A. Wei, Y. Lei, X. Cai, C.M. Li, Z.L. Dong, Appl. Phys. Lett. 88 (2006) 3106.
[17] S. Singh, S.K. Arya, P. Pandey, B. Malhotra, S. Saha, K. Sreenivas, V. Gupta, Bios 18 (2007) 21.
[18] S. Baruah, J. Dutta, Sci. Technol. Adv. Mater, 2016.
[19] X. Xu, M. Wu, M. Asoro, P. Ferreira, D. Fan, Cryst. Growth Des. 12 (2012) 4829–4833.
[20] J. Xie, P. Li, Y. Wang, Y. Wei, J. Phys. Chem. Solids 70 (2009) 112–116.
[21] F. Bai, P. He, Z. Jia, X. Huang, Y. He, Mater. Lett. 59 (2005) 1687–1690.
[22] X. Wang, J. Song, Z.L. Wang, J. Mater. Chem. 17 (2007) 711–720.
[23] V. Gressler, A.R. Franzen, G.J. de Lima, F.C. Tavernari, O.A. Dalla Costa, V. Feddern, J. Chromatogr. B 1015 (2016) 192–200.
[24] H. Wang, H. Jiang, H. Zhang, Y. Zhou, C. Wu, J. Zhao, C. Wu, L. Ba, X. Wang, J. Nanosci. Nanotechnol. 11 (2011) 1117–1122.
[25] W. Yu, X. Li, X. Gao, Cryst. Growth Des. 5 (2005) 151–155.
[26] T.-Q. Liu, O. Sakurai, N. Mizutani, M. Kato, J. Mater. Sci. 21 (1986) 3698–3702.
[27] W. L. Suchanek and R. E. Riman (2006).

[28] Y. Yang, H. Chen, B. Zhao, X. Bao, J. Cryst. Growth 263 (2004) 447–453.
[29] C. Chen, P. Liu, C. Lu, Chem. Eng. J. 144 (2008) 509–513.
[30] C. Li, Z. Yu, S. Fang, H. Wang, Y. Gui, J. Xu, R. Chen, J. Alloys Compd. 475 (2009) 718–722.
[31] Z. Siqingaowa, H. Yao, Front. Chem. Chin. 1 (2006) 277–280.
[32] R.J. Lauf, W. Bond, Am. Ceram. Soc. Bull. 63 (1984) (United States).
[33] A.K. Zak, M.E. Abrishami, W.A. Majid, R. Yousefi, S. Hosseini, Ceram. Int. 37 (2011) 393–398.
[34] S. Sepulveda-Guzman, B. Reeja-Jayan, E. de La Rosa, A. Torres-Castro, V. Gonzalez-Gonzalez, M. Jose-Yacaman, Mater. Chem. Phys. 115 (2009) 172–178.
[35] G. Tourillon, F. Garnier, J. Electroanal. Chem. Interfacial Electrochem. 135 (1982) 173–178.
[36] J.-M. Pernaut, J.R. Reynolds, J. Phys. Chem. B 104 (2000) 4080–4090.
[37] K. Jurewicz, S. Delpeux, V. Bertagna, F. Beguin, E. Frackowiak, Chem. Phys. Lett. 347 (2001) 36–40.
[38] C. Lin, B. Hwang, C. Lee, Mater. Chem. Phys. 55 (1998) 139–144.
[39] J.W. Goodwin, G.M. Markham, B. Vincent, J. Phys. Chem. B 101 (1997) 1961–1967.
[40] R. Najjar, S. Nematdoust, RSC Adv. 6 (2016) 112129–112139.
[41] W. Wei, L. Yuan, G. Hu, L.Y. Wang, J. Wu, X. Hu, Z.G. Su, G.H. Ma, Adv. Mater. 20 (2008) 2292–2296.
[42] R.A. Muzzarelli, Natural Chelating Polymers; Alginic Acid, Chitin and Chitosan, Pergamon Press, 1973.
[43] S. Ebrahimias, A. Zakaria, A. Kassim, S.N. Basri, Int. J. Nanomedicine 10 (2015) 217.
[44] E.G. Gozo, R.B. Yebes, CHEST Journal 86 (1984) 736–740.
[45] G. Falkay, L. Kovács, J. Perinat. Med. 14 (1986) 109–113 Official Journal of the WAPM.
[46] S.J. Kim, S.J. Park, S.I. Kim, React. Funct. Polym. 55 (2003) 53–59.
[47] N.A. Salahuddin, M. El-Kemary, E.M. Ibrahim, Nanosci. Nanotechnol. 5 (2015) 82–88.
[48] G.A. Mersal, M.M. Ibrahim, Int. J. Electrochem. Sci. 6 (2011) 761–777.
[49] R. White, Chromatography/Fourier Transform Infrared Spectroscopy and its Applications, CRC Press, 1989.
[50] G. Xiong, U. Pal, J. Serrano, K. Ucer, R. Williams, Phys. Status Solidi C 3 (2006) 3577–3581.
[51] T.C. Jagadale, S.P. Takale, R.S. Sonawane, H.M. Joshi, S.I. Patil, B.B. Kale, S.B. Ogale, J. Phys. Chem. C 112 (2008) 14595–14602.
[52] V. Parthasarathi, G. Thilagavathi, Int J Pharm Pharm Sci 3 (2011) 392–398.
[53] X.-G. Li, M.-R. Huang, L.-X. Wang, M.-F. Zhu, A. Menner, J. Springer, Synth. Met. 123 (2001) 435–441.
[54] S. Mansouri, P. Lavigne, K. Corsi, M. Benderdour, E. Beaumont, J.C. Fernandes, Eur. J. Pharm. Biopharm. 57 (2004) 1–8.
[55] F. Tian, Y. Liu, K. Hu, B. Zhao, Carbohydr. Polym. 57 (2004) 31–37.
[56] B. Guan, W. Ni, Z. Wu, Y. Lai, Sep. Purif. Technol. 65 (2009) 269–274.
[57] M.M. Abdi, A. Kassim, H.E. Mahmud, W.M.M. Yunus, Z.A. Talib, A.R. Sadrolhosseini, J. Mater. Sci. 44 (2009) 3682–3686.
[58] X. Wang, Y. Du, H. Liu, Carbohydr. Polym. 56 (2004) 21–26.
[59] M.E. Ganji, A. Bazargan, M. Keyanpour-Rad, M. Bahrevar, Funct. Mater. Lett. 3 (2010) 141–145.
[60] N. Izu, K. Shimada, T. Akamatsu, T. Itoh, W. Shin, K. Shiraishi, T. Usui, Ceram. Int. 40 (2014) 8775–8781.
[61] Q. Liu, L. Jiang, L. Guo, Small 10 (2014) 48–51 10.
[62] A. Kassim, H. Block, F.J. Davis, G.R. Mitchell, J. Mater. Chem. 2 (1992) 987–988.
[63] G. Mitchell, A. Geri, J. Phys. D. Appl. Phys. 20 (1987) 1346.
[64] A. Bazargan, F. Sharif, S. Mazinani, N. Naderi, J. Mater. Sci. Mater. Electron. (2017) 1–6.
[65] K.S. Sing, Pure Appl. Chem. 57 (1985) 603–619.
[66] W. Fan, M.A. Snyder, S. Kumar, P.-S. Lee, W.C. Yoo, A.V. McCormick, R.L. Penn, A. Stein and M. Tsapatsis, Nat. Mater. 7 (2008) 984–991.
[67] K. Sing, Pure Appl. Chem. 54 (1982) 2201–2218.
[68] Y.-Q. Li, S.-Y. Fu, Y.-W. Mai, Polymer 47 (2006) 2127–2132.
[69] X. Cui, J.F. Hetke, J.A. Wiler, D.J. Anderson, D.C. Martin, Sensors Actuators A Phys. 93 (2001) 8–18.
[70] C.E. Schmidt, V.R. Shastri, J.P. Vacanti, R. Langer, Proc. Natl. Acad. Sci. 94 (1997) 8948–8953.
[71] S. Kamalesh, P. Tan, J. Wang, T. Lee, E.T. Kang, C.H. Wang, J. Biomed. Mater. Res. 52 (2000) 467–478.
[72] S. Brunauer, L.S. Deming, W.E. Deming, E. Teller, J. Am. Chem. Soc. 62 (1940) 1723–1732.
[73] S. Lowell, J.E. Shields, M.A. Thomas, M. Thommes, Characterization of Porous Solids and Powders: Surface Area, Pore Size and DensitySpringer Science & Business Media 2012.